$\not{\ell}$-forbidden Gamow-Teller β decay of ^{57}Cu

D. R. Semon, M. C. Allen, H. Dejbakhsh, C. A. Gagliardi, S. E. Hale,* J. Jiang, L. Trache, R. E. Tribble, S. J. Yennello, H. M. Xu, and X. G. Zhou
Cyclotron Institute and Department of Physics, Texas A&M University, College Station, Texas 77843

B. A. Brown
Department of Physics and Astronomy and National Superconducting Cyclotron Laboratory, Michigan State University, East Lansing, Michigan 48824

(Received 10 August 1995)

Absolute branching ratios for the β decay of ^{57}Cu to excited states up to 3.3 MeV in ^{57}Ni have been determined, including the $\not{\ell}$-forbidden Gamow-Teller transition to the first excited state in ^{57}Ni. Four transitions to excited states at 0.768, 1.113, 2.443, and 3.007 MeV are observed in addition to the superallowed decay to the ground state of ^{57}Ni. The measured branching ratio to the ground state is 89.9 $\pm$ 0.8% and the branching ratios to the four excited states are 0.94 $\pm$ 0.09%, 8.6 $\pm$ 0.6%, 0.17 $\pm$ 0.03%, and 0.35 $\pm$ 0.04%, respectively. In addition we have measured the ^{57}Cu half-life and find it to be 196.3 $\pm$ 0.7 ms, which is in good agreement with the most recent measurement. B(GT) values have been extracted from the new results and are compared to shell model calculations.

PACS number(s): 23.40.−s, 21.60.Cs, 27.40.+z

I. INTRODUCTION

The nonrelativistic mean field approach to nuclear structure, as embodied in the nuclear shell model, has been quite successful in predicting the properties of low-lying states of nuclei. Extra-nucleonic effects, such as meson exchange currents and nucleon excitation into the $\Delta(1232)$ resonance, are not explicitly included in this approach to nuclear structure calculations. However, they are included implicitly when experimental data are used either as input into the calculations or to fit parameters. Consequently, it has been surprisingly difficult to find unambiguous signatures for these extra-nucleonic effects.

Adelberger *et al.* [1] pointed out that $\not{\ell}$-forbidden Gamow-Teller (GT) β decay is a sensitive way to determine the contribution to low-lying states from these extra-nucleonic effects. An $\not{\ell}$-forbidden GT decay is one that is allowed by the usual $\Delta J^{\Delta\pi}$ selection rules but is formally second-forbidden for the standard one-body operators acting on the single-configuration wave functions where the orbital angular momentum changes between the initial and final states. The problem is simplified when the parent and daughter states in the β decay can be represented as single-particle or -hole states outside of a closed shell. Even in these cases, the effect of core polarization can produce nonzero matrix elements from the normal one-body operators through the connection of multiparticle, multihole configurations in the parent and daughter nuclei. The only system where such an $\not{\ell}$-forbidden transition has been measured is in the decay of ^{39}Ca to an excited state in ^{39}K, [1,2] which is represented, in the single-particle shell model, by a $0d_{3/2}^{-1}\rightarrow 1s_{1/2}^{-1}$ transition.

The mirror nuclei, ^{57}Ni-^{57}Cu, offer another system where an $\not{\ell}$-forbidden GT decay can be measured for nuclei whose low-lying levels can be represented, to good approximation, as single-particle states. In the shell model, the low-lying levels in these nuclei are dominantly single-particle states built on the $N=Z$ nucleus ^{56}Ni which has the $0f_{7/2}$ shell filled. While this is not a shell closure associated with a principal quantum number, the strong spin-orbit coupling lowers the energy of the $0f_{7/2}$ orbital considerably relative to the $0f_{5/2}$ and $1p_{3/2}-1p_{1/2}$ orbitals, thus producing a large energy gap between them. The ground states of ^{57}Ni and ^{57}Cu are $1p_{3/2}$ states and the first two excited states in ^{57}Ni at 0.768 and 1.113 MeV are predominantly $0f_{5/2}$ and $1p_{1/2}$ configurations, respectively [3]. The dominant decay mode for ^{57}Cu is the superallowed ground state to ground state transition. Decays to both excited states in ^{57}Ni are allowed GT transitions by the usual angular momentum selection rules, but the $1p\rightarrow 0f$ transition is $\not{\ell}$-forbidden. Previous work on the γ decays and lifetimes of excited states in ^{57}Ni indicates that some configuration mixing is present for these levels [3,4]. Thus it will be necessary to have a large basis shell model calculation to account for this effect. The decay of ^{29}P to ^{29}Si is, in principle, similar to that of ^{57}Cu to ^{57}Ni, with ^{28}Si serving as the $0d_{5/2}$ closed shell core. However, the shell gap at $A=28$ is considerably smaller than for $A=56$ as indicated, for example, by the excitation energy of the first 2^+ state in each nucleus and the single-particle and -hole states in the neighboring nuclei. Consequently, ^{28}Si would be expected to represent a poorer approximation to a closed shell core than ^{56}Ni.

Prior to the work reported here, the extent of our knowledge of the decay of ^{57}Cu came from its measured mass excess [5–7] and two different determinations of its half-life. The first half-life measurement was done by detecting the β-delayed γ decay of the second excited state of ^{57}Ni and the second one was carried out by observing the β's, from a mass separated source, using plastic scintillator detectors.

*Present address: Department of Physics and Astronomy, University of North Carolina at Chapel Hill, Chapel Hill, NC 27599.

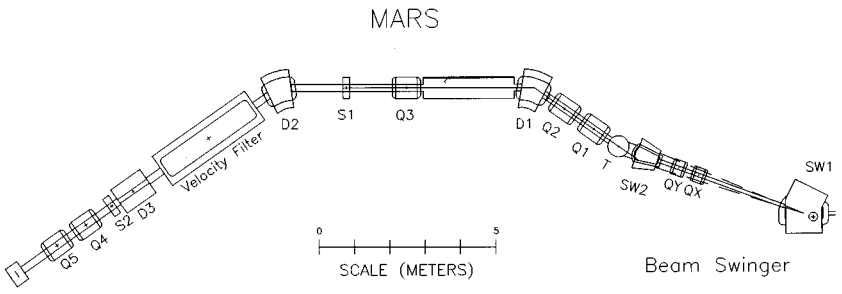

FIG. 1. A schematic layout of the recoil mass spectrometer MARS. The primary ^{58}Ni beam entered from the right, interacted in the cryogenic H_2 gas cell located at the center of the target chamber T, then stopped in a Faraday cup located beyond the dipole $D1$. The ^{57}Cu recoil nuclei were dispersed horizontally by $D1$. After passing through the energy selection slit located in front of the quadrupole $Q3$, they were deflected by $Q3$ and $D2$ to produce an achromatic beam at the entrance to the velocity filter. The velocity filter and $D3$ deflected the ^{57}Cu recoils vertically, producing a first-oder M/Q focus in the box located behind $Q5$. The various detector arrangements shown in Figs. 3, 5, and 7 were placed here.

The results of the two measurements were 233 $\pm$ 16 ms [8] and 199.4 $\pm$ 3.2 ms [9], with the more recent result differing from the earlier measurement by about two standard deviations. No experiment has been carried out with sufficient sensitivity to search for the ℓ-forbidden β decay. The branching ratio of the allowed GT decay to the 1.113 MeV state was estimated to be 3.7 $\pm$ 1.7% [8], by comparing the γ-ray yield to the β decay yield beyond the ^{54}Co end point, after using a time window to subtract the contribution to the observed β decay yield from ^{58}Cu.

We report below the first measurement of the absolute branching ratios for the decay of ^{57}Cu to several low-lying levels in ^{57}Ni, including allowed and ℓ-forbidden GT decays. In addition, a new half-life determination was made by directly measuring the positrons from the β decay. These measurements determine the ft values and hence the matrix elements for the decays. The results are compared to recent shell model calculations. The allowed GT decays provide new information about the quenching of GT strength in medium mass nuclei [10,11]. The implications on the role of extra-nucleonic effects in the transitions between low-lying nuclear states of these mirror nuclei are discussed.

II. GENERAL EXPERIMENTAL FEATURES

Three different measurements were performed to determine the transition strength of the ℓ-forbidden decay from the ground state of ^{57}Cu to the first excited state of ^{57}Ni: (1) the branching ratio for the ℓ-forbidden decay was obtained relative to the allowed GT decay that occurs to the second excited state of ^{57}Ni; (2) the absolute branching ratio for decay to the second excited state was determined; (3) the lifetime of ^{57}Cu was measured. Two other excited state branches were observed concurrently with the relative branching ratio measurements. Details of the individual measurements are discussed separately below.

All of the measurements were carried out with sources of ^{57}Cu that were obtained from the ^{1}H(^{58}Ni,^{57}Cu)2n reaction using primary ^{58}Ni^{17+} beams between 29 and 31 MeV/nucleon from the Texas A&M University K500 superconducting cyclotron. A H_2 gas cell, cooled to LN_2 temperature, was used as the primary production target. Havar entrance and exit windows of 5 μm thickness were glued onto standard stainless steel flanges with a cryogenic epoxy, which has a thermal expansion coefficient that closely matches that of stainless steel [12]. The window flanges were then attached to the body of the gas cell with standard copper gaskets. The windows were pressure tested to over 2000 torr. The gas cell typically was operated at about 760 torr, which, at 77 K, corresponds to a hydrogen target thickness of 2.8 mg/cm^2.

Using the cold gas cell at 760 torr as the target, ^{58}Ni^{28+} ions comprised less than 20% of the yield in the charge state distribution. The primary charge states were found to be 26^+ and 27^+, which had comparable yields. In contrast, over 80% of the beam was observed to be fully stripped when it passed through a 10 mg/cm^2 polyethylene target which resulted in a comparable energy loss for the beam as the gas cell. By adding a 1.5 mg/cm^2 Al foil after the Havar exit window, the yield of fully stripped ions increased to about 70% of the primary beam. The gas cell was thus run with this added stripper foil, so that the preponderance of the yield of ^{57}Cu recoils was in the 29^+ charge state.

Recoil ions were analyzed by the momentum achromat recoil spectrometer, MARS. A schematic layout of MARS is shown in Fig. 1. Detailed descriptions of the optics of MARS can be found elsewhere [13,14]. MARS was designed to be used for a wide range of reactions that utilize inverse kinematics. In the present set of experiments, MARS was operated at 0°. The reaction kinematics strongly focuses the recoil ions resulting in essentially 100% collection efficiency. The first three MARS quadrupoles, $Q1$, $Q2$, and $Q3$, along with the dipoles $D1$ and $D2$ form a momentum achromat. Recoil ions are dispersed in energy near the entrance to $Q3$ where an energy selection slit is located. $Q1$, $Q2$, and $D1$ produce a horizontal crossover near this point. In the present setup, the rigidity of the recoil ions was about 7% lower than that of the primary beam. A Faraday cup was offset from the central magnetic rigidity by the appropriate amount to intercept the fully stripped beam. The recoil ^{57}Cu ions were spread in energy by about 3%, primarily due to differential energy loss in the gas target. The energy selection slit in front of $Q3$ was set to transport essentially 100% of the ^{57}Cu recoil ions, but it was kept narrow to minimize the intensity of other recoil ions, notably ^{54}Co and ^{58}Cu, reaching the

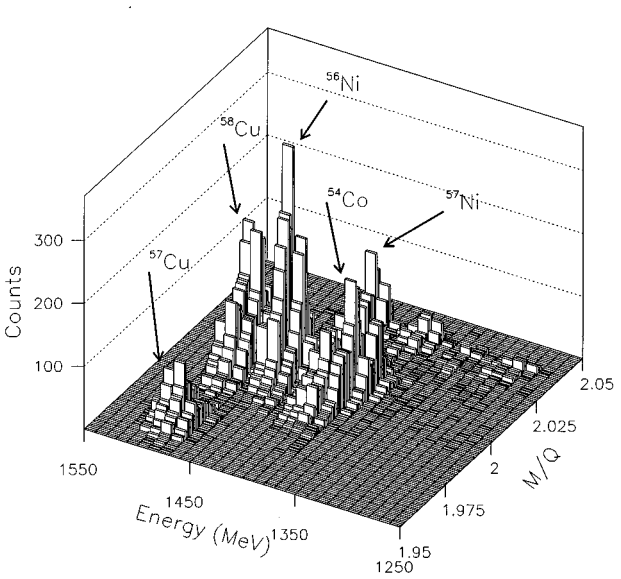

FIG. 2. A spectrum of energy vs position obtained in the Si strip detector at the MARS focal plane. The major particle groups are identified on the figure. A slit in front of the detector stopped other particles that were transported to the focal plane.

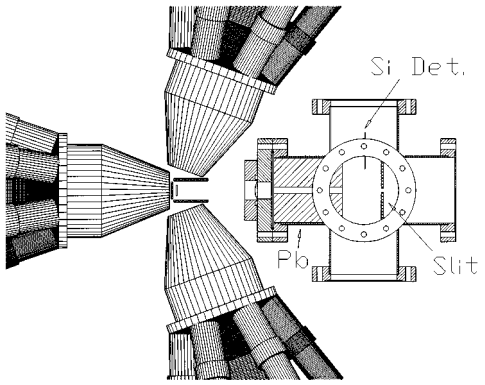

FIG. 3. The experimental setup that was used to measure the relative branching ratios for the decay of ^{57}Cu. The two plastic scintillators that formed the sides of the β detector box are not shown. See text for details regarding the detector hardware.

MARS focal plane. A mass analysis of the recoil ions occurs after the second magnetic dipole, $D2$. This part of MARS consists of a crossed electric and magnetic field velocity filter, which produces a vertical velocity dispersion around the central velocity, followed by a vertical bending magnet, $D3$, and two quadrupole magnets, $Q4$ and $Q5$. The action of $D3$, which was set to bend the recoil ions by about 5°, is to cancel the velocity dispersion from the velocity filter by producing a momentum dispersion with the opposite sign. The last two quadrupoles then focus the mass dispersed ions onto the MARS focal plane.

A position sensitive Si strip detector was used to detect the recoil ions at the focal plane. The detector was 1000 μm thick with an active area of 5 cm $\times$ 5 cm. It was mounted on a linear motion feedthrough so that it could be moved out of the beam and later reinserted into the beam without breaking vacuum. The front plane of the detector was segmented into 16 resistive strips. For each strip, one end was read out by a charge-sensitive preamplifier, while the opposite end was terminated by a 100Ω resistor. An energy signal was read out from the back plane of the detector. The position along a strip was determined from the ratio of the signal read out from a strip to the total energy signal. A spectrum of position versus particle energy is shown in Fig. 2. It is clear from the figure that the $^{57}Cu^{29+}$, with an $M/Q = 1.97$, is well isolated from the nearby groups with $N=Z$ and hence an $M/Q = 2.00$. The resulting mass resolution, expressed as $\delta M/M$, was 0.5% FWHM and the mass dispersion was 0.4 cm/(%$\delta M/M$). Three different recoil ion species are easily identified in the $N=Z$ group, ^{54}Co, ^{56}Ni, and ^{58}Cu. An adjustable slit was located at the MARS focal plane which could be set to transport a single particle group. After the MARS optics were tuned and the slit set, the Si detector was moved up out of the beam to a position behind the top slit. A lead collimator, through which the recoils passed, was placed behind the slit to reduce the yield of both photons and high energy positrons that were produced by activities stopped at the slit. The production and transport of recoils through MARS resulted in about 1 kHz of $^{57}Cu^{29+}$ for each particles nA of primary beam on target with a target thickness of 2.8 mg/cm^2.

III. DETERMINATION OF THE RELATIVE BRANCHING RATIO

The ^{57}Cu recoil ions that passed through the slit and lead collimator system described above exited the vacuum system through a 25 μm Kapton foil and were stopped in a 0.15 cm thick Al catcher foil. The slit was closed to about 5 mm, which allowed full transport of the ^{57}Cu recoils. A small number of $N=Z$ recoils were also allowed to pass through the slit. A β-γ coincidence experiment was set up to measure the rate of decays to the ℓ-forbidden first excited state of ^{57}Ni relative to the allowed Gamow-Teller decay to the second excited state. The layout of the detector system for this measurement is shown in Fig. 3. Five plastic scintillators, each of which were 3 mm thick and shaped to fit the geometric constraints imposed by the γ detectors, were placed around the catcher foil to form a five-sided box. Their geometric solid angle was over 90% of 4π sr. The thresholds for the outputs of the thin detectors were set for minimum ionizing electrons using a ^{90}Sr source. Three high purity Ge detectors from the HERA array [15] with 20% efficiency and Compton suppression were located just outside the plastic scintillators in a close geometry to optimize the solid angle coverage. Lucite cones were inserted into the front part of the Compton shields to prevent positrons from contaminating the Ge spectra.

The electronics for the measurement recorded coincidences from any β detector with any γ detector. Tennelec TC454 constant fraction discriminators were used to optimize the timing resolution of the plastic scintillators and Ge detectors. The coincidence time was recorded in a LeCroy LR2228 TDC, set on the 250 ps/channel range, with the β detector output providing the start signal for the TDC. Five TDC channels also were used as latches to identify which β detector was hit in each coincidence event. The analog signals from the Ge detectors were read out by an ORTEC

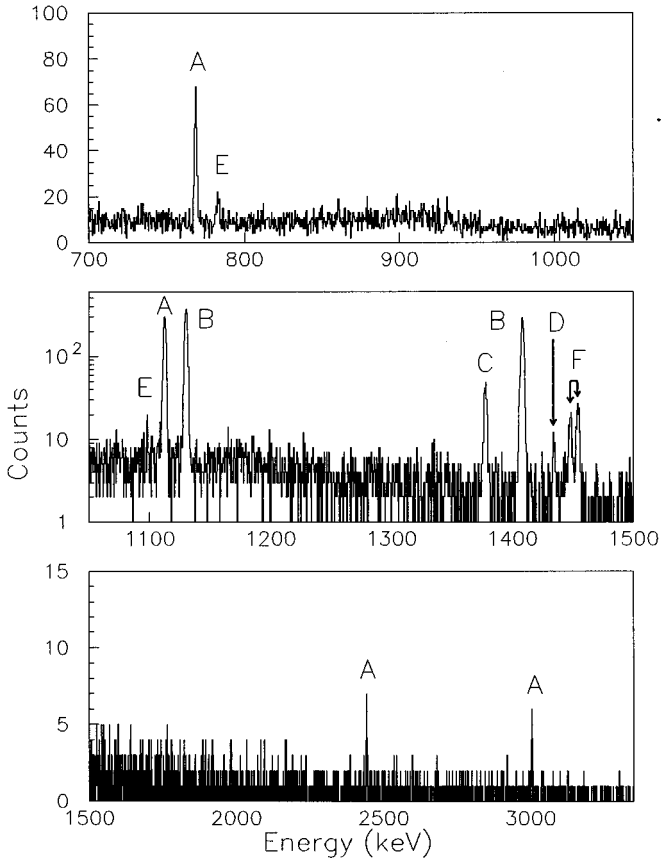

FIG. 4. A spectrum of γ rays in coincidence with β's from one of the three Ge detectors used in the determination of the relative branching ratios. The peaks marked on the spectrum correspond to decays from ^{57}Cu (A), ^{54m}Co (B), ^{57}Ni (C), ^{52m}Mn (D), ^{50m}Mn (E), and ^{58}Cu (F). Note that the top and bottom panels are shown with a linear scale, while the middle one is shown with a log scale.

AD413 ADC. Analog signals from the Compton shields were stored in an ORTEC AD811 ADC. Data acquisition was done by event mode recording using the Q system on a VAXstation. Software cuts on the Compton shield outputs were then used to optimize the signal to noise in the γ spectra.

The primary data for this measurement were obtained with a dc beam of ^{57}Cu recoils. The γ spectra were generated from the coincidence data after Compton suppression and coincidence timing cuts were imposed. An additional cut was made to exclude data in a Ge detector if the plastic scintillator in front of that detector was hit. This cut reduced the continuum background present in the Ge detectors due to positron Bremsstrahlung. It also minimized event losses, which could depend on β end point energy, due to positrons or annihilation radiation firing the Compton shields. The resulting spectrum of the γ yield in one of the detectors is shown in Fig. 4. The peaks corresponding to allowed GT decays (γ energies of 1.113, 2.443, and 3.007 MeV) and the $\not{\ell}$-forbidden GT decay (0.768 MeV) are indicated in the figure. Also indicated on the figure are lines from the decay of several $N=Z$ nuclei that passed through to the focal plane and a transition from the decay of ^{57}Ni, that built up from the decay of ^{57}Cu. The line from ^{52m}Mn occurs following the decay of ^{52}Fe. Both ^{52}Fe and ^{50m}Mn were produced off the gas cell windows.

Additional data were obtained using a pulsed beam in order to verify that the lifetime of the four transitions that were identified as coming from the decay of ^{57}Cu were indeed the same. Three time bins were used to store the data. Each bin was approximately 0.25 s in duration, corresponding to about 1 mean life for the ^{57}Cu decay. During the first time bin, the beam was on target and ^{57}Cu recoils were collected at the end of MARS. For the succeeding two time bins, the beam was removed by a deflector system located in the injection beam line between the electron cyclotron resonance ion source and the cyclotron. With the beam chopper on, there was no measurable beam current on the MARS Faraday cup, which corresponded to a beam on to beam off suppression factor of at least 10^4:1. The four peaks did show the expected decrease in yield across the second and third time bins consistent with them being ^{57}Cu decays. In contrast, the peaks due to ^{54m}Co, which has a half-life of 1.46 min, had nearly constant yield for all of the time bins.

Several background checks were carried out to verify that the observed γ-ray lines were not contaminated by background sources. The beam off β-γ coincidence rate from room background was found to be extremely low. The primary source for potential contamination in the spectra was background from β-delayed γ decays of recoil ions that were stopped by the focal plane slit. In order to determine the size of this background, a run was carried out with dc beam and the slit closed. The spectrum obtained from these running conditions was consistent with that expected from the reduced solid angle due to the source being stopped at the slit location. No spurious events were found in the spectra that would artificially enhance the yields for any of the ^{57}Cuγ-rays.

In order to determine the decay rate for the $\not{\ell}$-forbidden transition relative to the allowed GT transition, the yields to the two states from the β-γ coincidence data were corrected for the relative efficiencies of the Ge detectors and plastic scintillators at the different energies. The energy dependent efficiencies of the Ge detectors were determined using γ spectra from ^{152}Eu and ^{154}Eu, where the relative intensities of the lines are accurately known. The relative efficiency of the plastic scintillator box as a function of positron end point energy was estimated by a Monte Carlo calculation. Positrons were generated according to the standard allowed shape, with the Fermi function taken from [16]. Electromagnetic interactions were simulated using EGS4 [17]. The typical positron efficiency was found to be $\approx$50% after accounting for the reduced acceptance due to the veto on the scintillators in front of the Ge detectors. The relative scintillator efficiency was found to be 1.4 $\pm$ 2.0 % larger for transitions to the 0.768 MeV state and 16 $\pm$ 3 % lower for transitions to the 3.007 MeV state, compared to that for transitions to the 1.113 MeV state. Geometric effects make the largest contribution to the uncertainties in the relative efficiencies.

Including the data from both dc and pulsed beam running conditions and all three Ge detectors, we find the branching ratio to the 0.768 MeV state relative to the 1.113 MeV state to be 10.9 $\pm$ 0.6 %. The uncertainty in the result is dominated by the statistical precision and background in the yield

TABLE I. Branching ratios and ft values for the β decays of ^{57}Cu. The ^{57}Ni excitation energies and spin-parity assignments are from [3]. The relative branching ratios are measured with respect to the transition to the 1.113 MeV state in ^{57}Ni. The upper limits are 90% c.l. The uncertainties neglect any possible contributions from unobserved transitions to higher excited states above 3.3 MeV.

^{57}Ni final state		Branching ratio (%)		
J^π	E_x (MeV)	Relative	Absolute	ft value (s)
$\frac{3}{2}^-$	g.s.	–	89.9 ± 0.8	4671 ± 61
$\frac{5}{2}^-$	0.768	10.9 ± 0.6	0.94 ± 0.09	(2.73 ± 0.25)×10^5
$\frac{1}{2}^-$	1.113	100	8.60 ± 0.60	(2.35 ± 0.17)×10^4
$\frac{5}{2}^-$	2.443	2.0 ± 0.3	0.17 ± 0.03	(4.2 ± 0.7)×10^5
$\frac{7}{2}^-$	2.578	< 0.3	< 0.03	
$\frac{3}{2}^-$	3.007	4.1 ± 0.4	0.35 ± 0.04	(1.20 ± 0.15)×10^5
$\frac{7}{2}^-$	3.234	< 0.7	< 0.06	

to the ℓ-forbidden transition. A small contribution to the uncertainty (1.5%) is due to the determination of the relative efficiency of the Ge detectors at the two different energies. The same technique was used to determine the relative branching ratios of 2.0 ± 0.3 % and 4.1 ± 0.4 % for the decays to the states in ^{57}Ni at 2.443 and 3.007 MeV, respectively. In both cases, the uncertainties are dominated by our knowledge of the Ge detector efficiency at the higher energies relative to that at 1.113 MeV. No other transitions to states in ^{57}Ni below 3.3 MeV were observed, including the excited state at 3.234 MeV which has a 60% gamma decay branch via a cascade through the 0.768 MeV level [3]. This leads to upper limits of 0.3% and 0.7% (90% C.L.) for the relative branching ratios of the second-forbidden transitions to the 7/2$^-$ states at 2.578 and 3.234 MeV, respectively. Our results for the ^{57}Cu relative branching ratios to ^{57}Ni excited states are summarized in Table I.

IV. DETERMINATION OF THE ABSOLUTE BRANCHING RATIO

By determining the absolute branching ratio for the allowed GT decay to the second excited state of ^{57}Ni, the absolute branching ratio for the ℓ-forbidden decay can be obtained since the relative branching ratio between these two levels has been determined. The experimental setup that was used to measure the absolute branching ratio of the allowed decay is shown in Fig. 5. A pure source of ^{57}Cu was produced through MARS as described above, but the slit at the MARS focal plane was set at a width of 3 mm to pass only ^{57}Cu ions. A 5 cm × 1 cm × 500 μm thick rectangular Si solid state detector, located after the slit and lead collimator, was used to count the incoming ^{57}Cu ions. A Ge detector was placed directly behind the Si detector to count the γ rays from the ^{57}Cu source embedded in the Si detector.

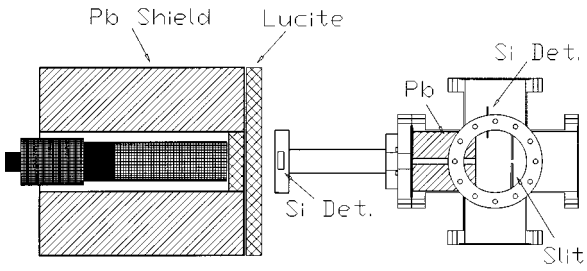

FIG. 5. The experimental setup that was used to measure the absolute branching ratio for the decay of ^{57}Cu to the 1.113 MeV excited state in ^{57}Ni.

The experiment was carried out by measuring the source strength with the Si detector and the yield of γ rays from the second excited state in ^{57}Ni in the Ge detector. Both detectors were operated in singles mode. No Compton suppression was used on the Ge detector, since positrons from the β decay could interact in the shield and hence veto real events. A cylindrical lead shield with a 3.81 cm inner radius and 6.5 cm thick wall was placed around the Ge detector in order to reduce the γ yield from room background. A 2.54 cm thick lucite plug was put in front of the detector inside of the shield. An additional 2.54 cm thick lucite plate was placed between the Ge detector/lead shield and the Si detector to stop positrons from the β decay. In order to reduce dead time in the data acquisition system, events in the Si detector were prescaled by a factor of 100 before they were stored in the computer. Typical readout rates during data acquisition were 11 and 35 Hz for the Si and γ detectors, respectively. The Si detector was set up so that it could be moved ±1 cm, in steps of 0.25 cm, along its narrow dimension to determine if any ^{57}Cu recoils were missing it or were hitting close to the edge, which could result in reduced pulse height due to incomplete charge collection in the detector. No yield was observed at either extreme of the settings, indicating that the source was fully contained in the Si detector. The effect of incomplete charge collection was obvious in the intermediate settings of the detector, but there was no evidence of incomplete charge collection when the detector was centered. In order to set limits on the horizontal extent of the source, Kapton degrader foils of varying thickness were added to cover the outside 1.5 cm of both ends of the detector. The energy loss through the foils was sufficient to easily distinguish recoil ions that passed through the center section from those that passed through one of the degrader sections. No events were observed corresponding to recoil ions that were outside the central 2 cm of the detector width. Also, no counts were observed in the Si detector that could be identified as ions coming from the strong $N=Z$ group which includes ^{58}Cu, ^{56}Ni, and ^{54}Co.

Figure 6 shows the spectrum obtained from the single Ge detector in the vicinity of the 1.113 MeV peak. Lines for both the 1.113 and 0.768 MeV decays in ^{57}Ni were observed in the singles spectrum. Other lines in the spectrum correspond to those from the decays of ^{50m}Mn, ^{54m}Co, and ^{58}Cu which were stopped at the slit, ^{57}Ni which built up in the Si detector during the run and room background. The ratio of yields in the two lines from the decay of ^{57}Cu is consistent with the results obtained in the relative branching ratio measurement, although the statistical precision is somewhat poorer. A beam on background run for the Ge detector was made with the slit at the focal plane closed in order to determine if any of the yield in the 1.113 MeV peak could be coming from activities stopped at the slit. This spectrum is also shown in Fig. 6. The background yield observed in the region of the 1.113 MeV γ ray was consistent with the rate

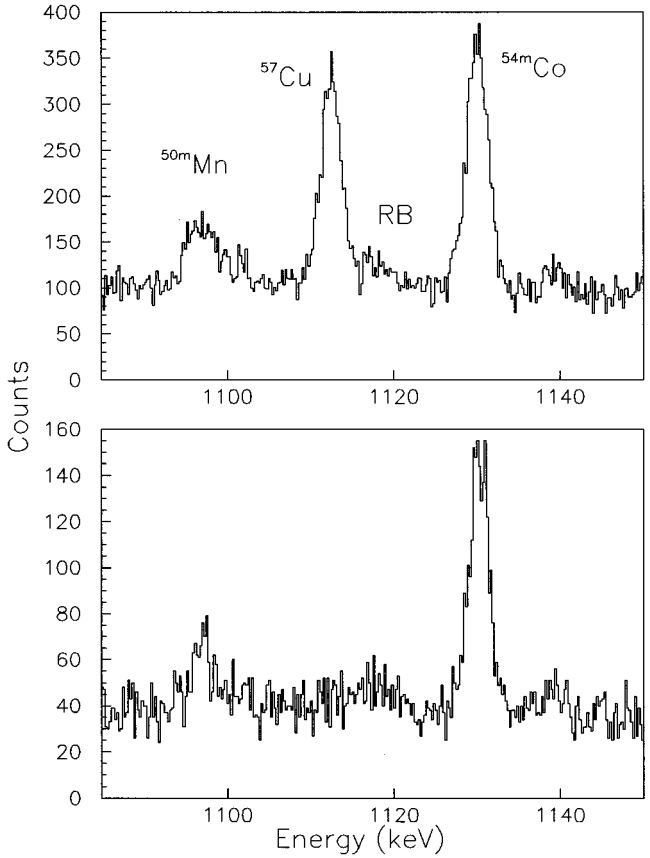

FIG. 6. A section of the γ-ray spectrum obtained for the determination of the absolute branching ratio of the decay of ^{57}Cu to the excited state at 1.113 MeV in ^{57}Ni. The top figure was obtained with the focal plane slit open and the bottom was with the slit closed (about 40% of the slit open running time). Peaks associated with ^{54m}Co and ^{50m}Mn decays on the slits, as well as room background (RB) from transitions in the Ra chain, are also noted.

of ^{57}Cu ions stopping at the focal plane slit, but with the severely reduced geometrical acceptance from the distant source. By contrast, the yields from the decays of the $N=Z$ ions, in particular the 1.130 MeV γ ray from ^{54m}Co, did not change when the slit was fully closed, further indicating that the $N=Z$ recoils did not contaminate the ^{57}Cu source in the Si detector. In measurements of the room background, no peaks were found under the 1.113 MeV γ-ray line, although lines from the Ra decay chain were seen nearby. The absolute efficiency of the Ge detector was obtained using a calibrated source which contained ^{152}Eu and ^{154}Eu. The γ rays in the source ranged from 0.080 to 1.596 MeV, thus spanning the region of interest. Since the ^{57}Cu recoil ions did not form a point source in the Si detector, efficiency measurements were made over a grid of positions to cover the full extent of the source of recoil ions. The absolute branching ratio for the allowed GT decay to the 1.113 MeV state in ^{57}Ni is found to be 8.6 $\pm$ 0.6 %. This uncertainty includes several contributions. The statistical uncertainty in the yield of the 1.113 MeV transition was 3%. The uncertainty in the determination of the Ge detector efficiency was 5% due to the source calibration. Finally, the observed yield was corrected by $+4 \pm 3$ % to account for pileup losses due both to Bremsstrahlung

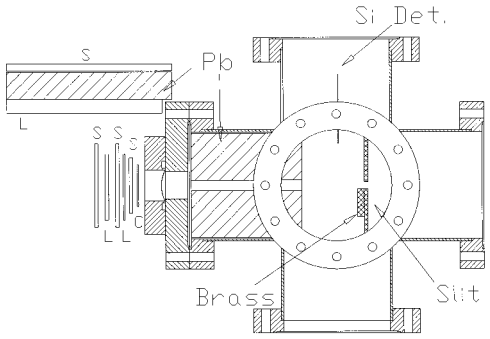

FIG. 7. The experimental setup that was used to measure the lifetime of ^{57}Cu. C indicates a 0.15 cm thick Al beam stop for the ^{57}Cu recoils. The plastic scintillators (S) and lucite absorbers (L) are also noted.

from the positrons as they stopped in the lucite in front of the Ge detector and 0.511 MeV γ rays.

V. DETERMINATION OF THE LIFETIME

The ^{57}Cu lifetime was determined by counting the β-decay rate as a function of time from a pure source. A schematic of the setup is shown in Fig. 7. The source was produced by allowing the ^{57}Cu to exit through a Kapton foil as described in Sec. III. The focal plane slit was once again set to pass only ^{57}Cu recoil ions (see Sec. IV for details). A 0.6 cm thick piece of brass was attached to the back of the lower slit to reduce the yield of high energy positrons from the decay of the $N=Z$ group at the slit. A three-element β detector telescope was set up using 3 mm thick plastic scintillator paddles. Absorber material was placed between the paddles to reduce the background due to coincidences of low energy β decays. A cosmic ray veto paddle was placed over the telescope to reduce the background rate. The veto paddle was shielded from the source by lucite and a lead brick. Data were obtained with both two- and three-detector coincidence requirements. The data from the two-detector setup had larger background but higher counting rates and ultimately produced a result with a sensitivity comparable to the three-detector telescope setup.

The ^{57}Cu source was produced with a pulsed beam that was obtained using the same deflector system which was described in Sec. III. A complete cycle consisted of beam on for 0.4 s and beam off for 2 s. The data for the lifetime were then obtained during the beam off part of the cycle by multiscaling the yield from the coincidences of the β detector telescope paddles. A PC based data acquisition system with a precision internal clock was used for multiscaling the data. The system was checked carefully for linearity and time response when it was used previously to measure several β-decay lifetimes [18]. The maximum coincidence count rate in the β detector telescope was 100 Hz, whereas the electronics dead time was $<$ 100 ns/event. Thus dead time effects in the scaling of the data were negligible. Results from the three-detector telescope data are shown in Fig. 8 along with a three-parameter fit; two parameters were used to represent the exponentially decaying source (lifetime and strength) and the third was set for a constant background.

A number of background checks were performed to verify

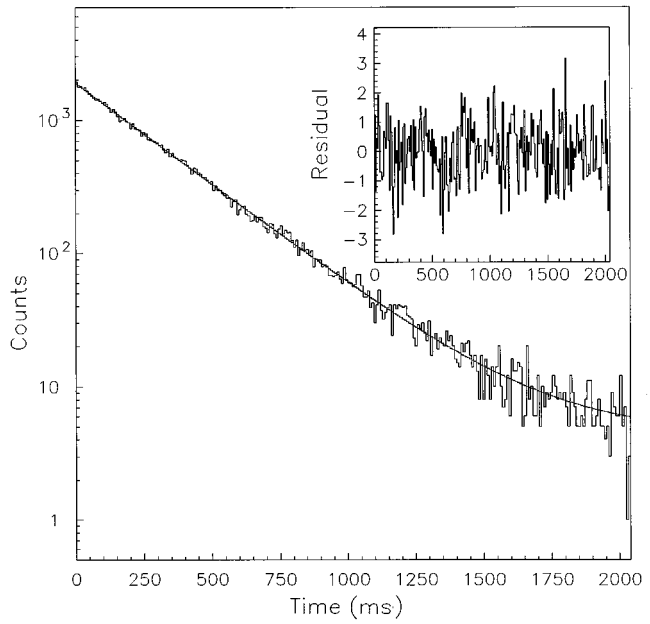

FIG. 8. The results of the triple-coincidence measurement of the ^{57}Cu lifetime. The solid line represents a three-parameter fit to the data, including a decaying exponential and a constant background. The residuals shown in the inset represent the differences between the fit and the data.

that the data were not contaminated by other short lived activities or the build-up of longer lived β emitters. The event rate was checked periodically with the beam off. No indication of a change in this background rate was observed. Thus, the system was effectively discriminating against the low energy β's from the decay of ^{57}Ni, which has a 35.6 h half-life [19,20]. The beam pulse period was changed to 4 s beam on and 16 s beam off to look for decays with lifetimes somewhat longer than those of ^{57}Cu. No evidence was seen in the data for other components in the decay. Runs with the focal plane slit closed produced a spectrum with a yield slightly above the room background. The rates and spectrum were consistent with room background plus ^{57}Cu from a distant source. Finally, MARS was retuned to pass the $N=Z$ group through the slit. The resulting spectrum had a much different character and showed evidence for decays of ^{58}Cu, ^{54}Co, and ^{54m}Co, which have half lives of 3.20 s, 0.193 s, and 1.46 min, respectively.

The lifetime that we determine for ^{57}Cu is 196.3 $\pm$ 0.7 ms, which is a combination of the lifetimes from the two detector run (195.0 $\pm$ 1.1 ms, χ^2_ν=0.86) and the three-detector run (197.0 $\pm$ 0.8 ms, χ^2_ν=1.02). The uncertainty in the result is dominated by the statistical precision of the first few channels in the decay curve relative to the background. Combining this with the previous measurement that utilized a mass separated source [9], we find a new lifetime of 196.4 $\pm$ 0.7 ms. We adopt this value below when calculating experimental transition strengths.

VI. RESULTS AND DISCUSSION

The results from the measurements described in Secs. III and IV can be combined to provide absolute branching ratios for the decay of ^{57}Cu to the ground state and low-lying excited states in ^{57}Ni. These branching ratios are summarized in Table I. The result quoted for the ground state is based on the assumption that there is no significant missing β-decay strength to levels in ^{57}Ni above 3.3 MeV. Similarly, the results for the excited states assume that they have no significant cascade feeding from unobserved β decays to higher excited states in ^{57}Ni. The new lifetime and branching ratios are used to determine the ft values for the decays which are quoted in Table I. The phase space factors for the various transitions were calculated from the tables of [21], which assume an allowed GT shape and include the $O(\alpha)$ outer radiative corrections, and a ground state Q_{EC} of 8.769 $\pm$ 0.014 MeV, the weighted average from [5–7].

Using the ft values from Table I, the B(GT) values for the decays have been deduced, as given in Table II. The ft value is related to the transition strength by

$$ft=\frac{6146\ \text{s}}{(g_A/g_V)^2B(\text{GT})+B(F)} \tag{1}$$

with $|g_A/g_V|$=1.260 [22,23]. $B(F)$ is the reduced matrix element of the $\tau_\pm$ Fermi operator which only connects isobaric analog states if isospin is conserved. The precision of the experimental ft value for the transition to the ^{57}Ni ground state required us to make a number of corrections when calculating its B(GT) value. The isospin mixing correction to the Fermi matrix element was calculated within a single-particle model, using the methods discussed in [24,25]. In particular, we calculated the Hartree-Fock radial wave functions for the valence $p_{3/2}$ proton and neutron using the Skyrme M^* interaction [26]. The correct asymptotics were enforced by adjusting the HF potential depth to reproduce the experimental proton and neutron separation energies of ^{57}Cu and ^{57}Ni, respectively. The overlap of the proton and neutron radial wave functions obtained with this calculation gave δ_{RO}=1.4%. The small proton separation energy of ^{57}Cu, S_p = 695 keV, makes this correction much larger than inferred from an extrapolation of the calculations for the well-known $0^+\rightarrow 0^+$ β decays (see [27] for a review). In this simple model, the valence ''isospin mixing'' correction to $B(F)$ is zero. A recent calculation for the $0^+\rightarrow 0^+$ decay of ^{58}Zn, which involves the same orbitals as the ^{57}Cu to ^{57}Ni ground state transition, concluded that valence isospin mixing reduces $B(F)$ by an additional 0.2% [25]. Therefore, we calculated the B(GT) for the analog transition to the ^{57}Ni ground state with the assumption that its Fermi strength is $B(F)=0.984\pm 0.006$, where the uncertainty reflects the difference between calculations of the radial overlap using Hartree-Fock and Woods-Saxon wave functions [25]. We also included a 0.57% correction to the analog transition ft value to account for $O(Z\alpha^2)$ and $O(Z^2\alpha^3)$ radiative corrections [28].

Shell model calculations for $A=57$ were carried out in the fp model space in which the $0f_{7/2}$, $0f_{5/2}$, $1p_{3/2}$, and $1p_{1/2}$ orbitals are active. We used the FPD6 effective interaction [29] which was obtained from a fit of six potential parameter strengths and four single-particle energies to binding energies and excitation energies of fp shell nuclei with mass $A=41-49$, for which full space calculations can be carried out. While it has recently become possible with the Monte

TABLE II. Comparison of shell model results with energy levels and Gamow-Teller decay strengths in $A=29$ and 57. The experimental results for $A=29$ are from [10], while those for $A=57$ are from this work. Excitation energies are in MeV.

				Calculated E_x		B(GT)				
A	J_i	J_f	E_x	3p-2h	Full	1p-0h	3p-2h	Full	Effective [a]	Expt.
29	$\frac{1}{2}^+$	$\frac{1}{2}^+$	0	0	0	3.000	1.266	0.219	0.150	0.169(8)
		$\frac{3}{2}^+$	1.27	1.00	1.39	0	0.003	0.026	0.020	0.060(1)
		$\frac{1}{2}^+$	2.43	6.49	2.63	0	0.113	0.559	0.274	0.256(8)
57	$\frac{3}{2}^-$	$\frac{3}{2}^-$	0	0		1.667	0.344		0.214	0.204(12)
		$\frac{5}{2}^-$	0.77	1.08		0	0.017		0.013	0.014(1)
		$\frac{1}{2}^-$	1.11	0.97		1.334	0.185		0.101	0.164(12)
		$\frac{5}{2}^-$	2.44	4.13		0	0.012		0.006	0.009(2)
		$\frac{3}{2}^-$	3.01	4.71		0	0.012		0.007	0.032(4)
		$\frac{5}{2}^-$		4.82		0	0.077		0.042	
		$\frac{3}{2}^-$		5.10		0	0.048		0.025	

[a]The results in this column were obtained with the effective GT operator from the row labeled ''all GT decay'' in Table 2 of [32].

Carlo shell model method to carry out full space calculations for nuclei near $A=57$ [30], at present the method can only be applied to even-even ground states. Thus, in order to make the calculations feasible for $A=57$, the full fp model space (with dimensions of the order of 10^7) must be truncated. We will compare the experimental results to those obtained from the extreme single-particle model in which the $0f_{7/2}$ orbital is completely filled (the 1p-0h model) and from a more extended model in which one or two nucleons are allowed to be excited from the $0f_{7/2}$ orbital (the 3p-2h model). The only change made in the FPD6 interaction to extend it from the full-space $A=41-49$ region to the truncated-space $A=57$ case was to readjust the single-particle energies to reproduce the observed energies of the $0f_{7/2}$ single-hole state and $0f_{5/2}$, $1p_{3/2}$, and $1p_{1/2}$ single-particle states relative to a closed $0f_{7/2}$ shell. The adjusted FPD6 interaction has been used to describe successfully the low-lying $E2$ strength in ^{56}Ni and neighboring nuclei [31].

In Tables II and III we compare the experimental B(GT) and $B(M1)$ values with those calculated. The agreement between the calculated and measured B(GT)'s is remarkably good, in contrast to the results for the measured and calculated values for the ℓ-forbidden $M1$ transition. Also included in Tables II and III is a comparison of the data for the $A=29$, $T=1/2$ GT and $M1$ transitions. As we noted in the Introduction, the structure of $A=29$ is analogous to the present case of $A=57$, with the $0f_{7/2}$ core replaced by $0d_{5/2}$ and the valence $0f_{5/2}$, $1p_{3/2}$, and $1p_{1/2}$ orbitals replaced by $0d_{3/2}$ and $1s_{1/2}$. In the 1p-0h limit the allowed single-particle transitions are $1s_{1/2}$ to $1s_{1/2}$ for $A=29$ and $1p_{3/2}$ to $1p_{3/2}$ and $1p_{1/2}$ for $A=57$. The ℓ-forbidden transitions are $1s_{1/2}$ to $0d_{3/2}$ for $A=29$ and $1p_{3/2}$ to $0f_{5/2}$ for $A=57$. Configuration mixing up to 3p-2h results in a large reduction of the allowed transitions and a small but nonzero value for the ℓ-forbidden transitions. For $A=29$ one can carry out the calculations in the full sd shell-model space, where one finds a further reduction in the allowed transitions and somewhat larger ℓ-forbidden transition strengths. The experimental results for $A=29$ are in reasonable agreement with the full space calculation.

For the sd shell nuclei, there is also evidence for configuration mixing beyond the sd model space, as well as meson exchange current effects [32]. These can be accounted for

TABLE III. Comparison of shell model results with $M1$ decay strengths (in μ_N^2) and magnetic moments in $A=29$ and 57.

			$B(M1)$ or magnetic moment				
A	J_i	J_f	1p-0h	3p-2h	Full	Effective[a]	Expt.
29	$\frac{3}{2}^+$	$\frac{1}{2}^+$	0	0.0005	0.012	0.029	0.063(2)[b]
57	$\frac{5}{2}^-$	$\frac{3}{2}^-$	0	0.0017		0.012	0.026(3)[c]
	$\frac{1}{2}^-$	$\frac{3}{2}^-$	2.33	0.258		0.16	0.27(6)[c,d]
^{29}Si μ	$\frac{1}{2}^+$		-1.913	-1.226	-0.501	-0.566	-0.555[e]
^{29}P μ	$\frac{1}{2}^+$		2.793	1.974	1.101	1.201	1.235[e]
^{57}Ni μ	$\frac{3}{2}^-$		-1.913	-0.628		-0.71	$(-)0.88(6)$[e]
^{57}Cu μ	$\frac{3}{2}^-$		3.79	2.45		2.48	

[a]The results in this column were obtained with the effective $M1$ operator from the row labeled ''moments plus $M1$ decay'' in Table 2 of Ref. [32].

[b]Reference [34].

[c]Reference [3].

[d]Assumes the transition is pure $M1$.

[e]Reference [35].

phenomenologically by the introduction of effective GT and $M1$ one-body operators, two of which renormalize the spin and orbital operators (δ_s and δ_l) and another (proportional to δ_p) which involves a new operator of the form $[Y^{(2)}\otimes\sigma]_{J=1}$. This latter operator allows for the $\not\ell$-forbidden $M1$ and GT single-particle transitions to be nonzero. Empirical values of the parameters δ_s, δ_l, and δ_p have been obtained from a fit to the B(GT), $B(M1)$ and magnetic moment data in the sd shell (see Table II of [32]), which include among them the $\not\ell$-forbidden transition in $A=39$ [1,2]. These empirical parameters have been compared to microscopic calculations of the configuration mixing and exchange current contributions [32,33]. In order to evaluate whether these parameters also represent an appropriate effective operator for the fp shell, they have been used to obtain the results labeled ''effective'' in Tables II and III. In each case, the effective interaction has been applied to the full sd shell model wave functions for the $A=29$ calculations and to the 3p-2h fp shell model wave functions for the $A=57$ calculations. The main effect of the higher-order configuration mixing is to quench the strength of the allowed GT transitions to about 60% of the value calculated within the fp shell. The effect of δ_p turns out to be small for the GT transitions, but it is important for the $M1$ transitions, bringing the $\not\ell$-forbidden strength up an order of magnitude and into much better agreement with experiment. We remark, however, that the δ_p value which is needed to reproduce the $\not\ell$-forbidden $M1$ transitions is in particularly poor agreement with the microscopic calculations [1,2,32,33], it is about a factor of 4 larger than expected.

VII. CONCLUSION

We have measured the lifetime of ^{57}Cu and determined the branching ratios for both allowed and $\not\ell$-forbidden β decay to excited states up to 3.3 MeV in ^{57}Ni. The resulting B(GT) values, including that for the $\not\ell$-forbidden decay, are in good agreement with the results from an fp shell model calculation which includes 3p-2h configuration mixing. Thus no additional extra-nucleonic effects are needed to understand the results. In contrast, the experimental $\not\ell$-forbidden $M1$ strength is much larger than the prediction. This same behavior has been observed in both $A=29$ and $A=39$. In those cases, the agreement with experiment was improved substantially when effective one-body operators were added to the normal GT and $M1$ operators to account for the effects of meson exchange currents and configuration mixing outside the sd shell. We find the same effective one-body operators improve the agreement between theory and experiment in $A=57$ as well. However, the δ_p contribution needed to obtain agreement with the observed $\not\ell$-forbidden $M1$ transitions is substantially larger than expected based on microscopic calculations. Thus, while the $\not\ell$-forbidden β decay is adequately described by the shell model, $\not\ell$-forbidden $M1$ transitions are still relatively poorly understood theoretically [32,33]. More precise measurements of the $\not\ell$-forbidden $M1$ matrix elements in $A=57$, including the analog transition in ^{57}Cu, may help resolve this discrepancy.

ACKNOWLEDGMENTS

We would like to acknowledge F. Stephens of the Lawrence Berkeley Laboratory for his assistance in the loan of the Compton-suppressed Ge detectors from the HERA array and C. Baktash of Oak Ridge National Laboratory for the loan of the automatic LN_2 fill system that was used with the Ge detectors. This work was supported in part by the U.S. Department of Energy under Grant No. DE-FG03-93ER40773, the National Science Foundation under Grant No. PHY-94-03666, and by the Robert A. Welch Foundation.

[1] E.G. Adelberger, J.L. Osborne, H.E. Swanson, and B.A. Brown, Nucl. Phys. **A417**, 269 (1984).

[2] E. Hagberg, T.K. Alexander, I. Neeson, V.T. Koslowsky, G.C. Ball, G.R. Dyck, J.S. Forsert, J.C. Hardy, J.R. Leslie, H.-B. Mak, H. Schmeing, and I.S. Towner, Nucl. Phys. **A571**, 555 (1994).

[3] M.B. Bhat, Nucl. Data Sheets **67**, 195 (1992).

[4] C.R. Gould, D.P. Balamuth, P.F. Hinrichsen, and R.W. Zurmühle, Phys. Rev. **188**, 1792 (1969).

[5] C.A. Gagliardi, D.R. Semon, R.E. Tribble, and L.A. Van Ausdeln, Phys. Rev. C **34**, 1663 (1986).

[6] E. Stiliaris, H.G. Bohlen, X.S. Chen, B. Gebauer, A. Miczaika, W. von Oertzen, W. Weller, and T. Wilpert, Z. Phys. A **326**, 139 (1987).

[7] B. Sherrill, K. Beard, W. Benenson, C. Bloch, B.A. Brown, E. Kashy, J.A. Nolen, Jr., A.D. Panagiotou, J. van der Plicht, and J.S. Winfield, Phys. Rev. C **31**, 875 (1985).

[8] T. Shinozuka, M. Fujioka, H. Miyatake, M. Yoshii, H. Hama, and T. Kamiya, Phys. Rev. C **30**, 2111 (1984).

[9] H. Hama, T. Shinozuka, M. Fujioka, M. Yoshii, K. Taguchi, and T. Ishimatsu (unpublished).

[10] B.A. Brown and B.H. Wildenthal, At. Data Nucl. Data Tables **33**, 347 (1985). The $B(\mathrm{GT})_{BW}$ used in this paper is related to the ft value by $ft = 6170/[B(\mathrm{GT})_{BW}+B(F)]$ and, thus, $B(\mathrm{GT})_{BW}=(g_A/g_V)^2B(\mathrm{GT})$.

[11] E. Caurier, A.P. Zucker, A. Poves, and G. Martinex-Pinedo, Phys. Rev. C **50**, 225 (1994).

[12] Eccobond 27 from Emerson and Cuming, Inc.

[13] R.E. Tribble, R.H. Burch, and C.A. Gagliardi, Nucl. Instrum. Methods A **285**, 441 (1989).

[14] R.E. Tribble, C.A. Gagliardi, and W. Liu, Nucl. Instrum. Methods B **56/57**, 956 (1991).

[15] R.M. Diamond, *Instrumentation for Heavy Ion Nuclear Research*, edited by D. Shapira (Harwood Academic, New York, 1985), p. 259.

[16] H. Behrens and J. Jänecke, *Numerical Tables for Beta-Decay and Electron Capture*, Landolt-Börnstein Numerical Data and Function Relationships in Science and Technology, Group I, Vol. 4, edited by K.-H. Hellwege (Springer-Verlag, Berlin, 1969).

[17] W.R. Nelson, H. Hirayama, and D.W.O. Rogers, ''The EGS4 Coding System,'' SLAC Report No. 265, 1985, unpublished.

[18] R.H. Burch, Jr., C.A. Gagliardi, and R.E. Tribble, Phys. Rev. C **38**, 1365 (1988).
[19] J.K. Dickens, J. Radioanal. Nucl. Chem. **103**, 273 (1986).
[20] A. Grutter, Int. J. Appl. Radiat. Isotop. **33**, 533 (1982).
[21] D.H. Wilkinson and E.F. Macefield, Nucl. Phys. **A232**, 58 (1974).
[22] G. Savard, A. Galindo-Uribarri, E. Hagberg, J.C. Hardy, V.T. Koslowsky, D.C. Radford, and I.S. Towner, Phys. Rev. Lett. **74,** 1521 (1995).
[23] E. Klemt, P. Bopp, L. Hornig, J. Last, S.J. Freedman, D. Dubbers, and O. Schärpf, Z. Phys. C **37**, 179 (1988).
[24] W.E. Ormand and B.A. Brown, Phys. Rev. Lett. **62**, 866 (1989).
[25] W.E. Ormand and B.A. Brown, Phys. Rev. C **52**, 2455 (1995).
[26] J. Bartel, P. Quentin, M. Brack, C. Guet, and H.-B. Hakansson, Nucl. Phys. A386, 79 (1982).
[27] J.C. Hardy, I.S. Towner, V.T. Koslowsky, E. Hagberg, and H. Schmeing, Nucl. Phys. **A509**, 429 (1990).
[28] A. Sirlin, Phys. Rev. D **35**, 3423 (1987).
[29] W.A. Richter, M.G. Van der Merwe, R.E. Julies, and B.A. Brown, Nucl. Phys. **A523**, 325 (1991).
[30] D.J. Dean, P.B. Radha, K. Langanke, Y. Alhassid, S.E. Koonin, and W.E. Ormand, Phys. Rev. Lett. **72**, 4066 (1994). The FPD6 interaction is referred to as the ‘‘Brown-Richter’’ interaction in this paper.
[31] G. Kraus *et al.*, Phys. Rev. Lett. **73**, 1773 (1994).
[32] B.A. Brown and B.H. Wildenthal, Nucl. Phys. **A474**, 290 (1987).
[33] I.S. Towner, Phys. Rep. **155**, 263 (1987).
[34] P.M. Endt and C. van der Leun, Nucl. Phys. **A521**, 1 (1990).
[35] P. Raghavan, At. Data Nucl. Data Tables **42**, 189 (1989).